Universal Scherrer Equation for Graphene Fragments

Daniel J. Lim,[1] Nigel A. Marks,[1] and Matthew R. Rowles[2,*]

[1] *Department of Physics and Astronomy, Curtin University, Perth WA 6102, Australia*
[2] *John de Laeter Centre, Curtin University, Perth WA 6102, Australia*

(Dated: February 6, 2020)

Graphene fragments spanning a wide range of size and shape were studied computationally using the Debye scattering equation. The calculated diffraction patterns were analyzed using the Scherrer equation to infer the fragment size, L_a. Comparison with the known fragment sizes reveals a strong affine relationship between L_a and the Scherrer quantity $\lambda/(B\cos\theta)$. To preserve this relationship, we propose modifying the Scherrer equation to include an empirical additive constant. Our approach solves the well-known problem of size-dependence in the shape factor and yields a universal expression by defining L_a as the square-root of the fragment area. The relationship between observed diffraction peak positions and unit cell parameters is also discussed.

I. INTRODUCTION

The determination of layer size is an important task for the characterisation of many classes of carbon materials such as carbon blacks, glassy carbon, graphite, and graphene. While Raman spectroscopy is a popular non-destructive technique for layer size determination [1], the most accurate bulk values are obtained from powders using X-ray diffraction. Analysis of diffraction patterns involves the use of the Scherrer equation,

$$L = \frac{K\lambda}{B\cos\theta} \tag{1}$$

which connects the width, B, and position, θ, of a diffraction peak to the physical size of the crystallite, L, via the wavelength, λ, and a dimensionless constant, K. While there is no unique choice, the (002) peak is commonly used to determine the crystallite size in the prismatic direction (L_c), while the (10) and (11) peaks are popular choices to determine size in the basal plane (L_a).

The most important parameter in the Scherrer equation is the quantity K, also known as the shape factor. In 1918, Scherrer [2] derived a general value of K=0.94, while the first derivation of a shape factor specific for carbon was by Warren in 1941 [3], who proposed using K=1.84 for L_a. This value, which was calculated using rhombus-shaped fragments, remains in common use. Another widely-used shape factor is K=0.89, which was derived by WL Bragg [4] and first used for carbon L_c values by Biscoe & Warren [5]. In later work, Warren and Bodenstein [6] performed analysis on circular fragments and proposed K=1.77 for L_a. The choice of K was again revisited in 2004 by Iwashita *et al.* [7] who performed inter-laboratory tests and suggested a single universal value of K=1 for all crystallite directions. In a separate article, Warren and Bodenstein [8] also reported a further complexity whereby the L_a shape-factor is size-dependent, varying from 1.1 up to 2.0. This leads to a circular argument whereby K depends on L_a, which in turn depends on K. This problem was recently examined by Fujimoto [9], Dopita *et al.* [10] who used the Debye scattering equation [11] to study stacked graphitic layers of varying size and shape. Both studies noted a significant size-dependence for small fragments with $L_a \lesssim 100$ Å.

Another complexity in using the Scherrer equation is the meaning of the quantity L. While it is unambiguous how to define L_c, this being simply the number of layers multiplied by the interlayer spacing, the definition of L_a is more problematic. The original 1941 paper by Warren defines L_a in an opaque manner via the formula

$$L_a = \left[\left(\frac{\mathbf{b}_1\cdot\hat{\mathbf{G}}}{N_1}\right)^2 + \left(\frac{\mathbf{b}_2\cdot\hat{\mathbf{G}}}{N_2}\right)^2\right]^{-\frac{1}{2}} \tag{2}$$

where $\mathbf{b}_1$ and $\mathbf{b}_2$ are the hexagonal in-plane reciprocal lattice vectors, N_1 and N_2 are the number of unit-cells in real space and $\mathbf{G}$ is a unit-vector parallel to the reflection of interest. In their 1966 article, Warren and Bodenstein note that Eq. 2 is equivalent to the definition $L_a = Na\times\sqrt{3}/2$ where Na is the side-length of a 60° rhombus. In the same article, they introduce a new definition of L_a for a circular fragment, defining it as the ratio of the area to the diameter, yielding the expression $L_a = R\times\pi/2$, where R is the radius of the fragment. Another measure of layer size was proposed by Diamond [12] who introduced the expression $L_a = 1.768\sqrt{N}$, where N is the number of atoms in the layer. In 2002, Ruland and Smarsly [13] proposed a completely general definition of L_a employing a series of integrals involving distributions of chord lengths, while a recent study by Puech *et al.* [14] defined L_a as the diameter of circular fragments.

In this work we revisit the Scherrer equation using a large set of graphene fragments of varying shape and size. Using the Debye scattering equation and an intuitive area-based definition of L_a, we identify a strong affine correlation between L_a and the quantity $\lambda/(B\cos\theta)$ defined in Eq. 1. Based on this observation, we introduce a modified Scherrer equation which includes a small additive constant. This new form eliminates almost all of the size-dependence, is independent of the diffraction peak, and works equally well for a variety of regular polygons.

* Corresponding author. Email: matthew.rowles@curtin.edu.au

II. METHODOLOGY

Following in the spirit of Diamond [12], we define L_a using the area of a graphene fragment, via the expression:

$$L_a = \sqrt{\text{area}} \tag{3}$$

This form is easy to interpret: for a square fragment L_a is just the side length, while for other regular shapes a simple relationship can be determined. For example, a circle of diameter D has $L_a = D \times \sqrt{\pi}/2 \approx 0.89D$ while a 60° rhombus of side-length D has $L_a = D \times (3/4)^{1/4} \approx 0.93D$. Using these geometric factors, it is straightforward to convert common literature values of the Scherrer shape factor to their Eq. 3 equivalents: K=1.84 for a rhombus becomes 1.98, while K=1.77 for a circle becomes 2.00. Assuming a graphene lattice parameter of 2.46 Å, Eq. 3 can also be written in the equivalent form $L_a = 1.618\sqrt{N}$ where N is the number of atoms and L_a is in ångströms. With this expression, fragments of arbitrary shape can be easily categorized without recourse to complicated definitions.

Ideal graphene fragments of varying shape (circular, hexagonal, square, rhombus and elliptical; see Fig. 1) and size ($L_a \approx$ 25–690 Å) were generated by tiling a two-dimensional unit cell of length 2.46 Å, internal angle 120°, and containing two carbon atoms at fractional coordinates $\left(\frac{1}{3}, \frac{2}{3}\right)$ and $\left(\frac{2}{3}, \frac{1}{3}\right)$. No attempt was made to introduce curvature, dislocations, or to minimise the energy of the structure. The eccentricity of the ellipses is defined as $\varepsilon = \sqrt{1 - b^2/a^2}$, where a and b are the semi-major and semi-minor axes, respectively. For the rhombus, a and b are defined as the long and short diagonals, respectively, while the regular polygons all have an eccentricity of zero.

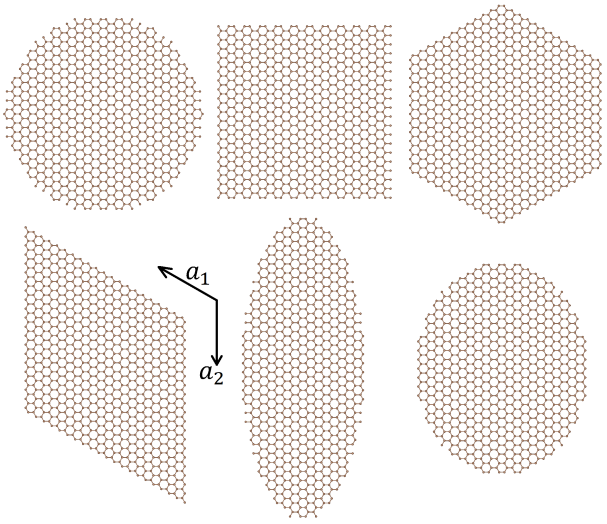

FIG. 1. The six types of graphene fragments used to calculate diffraction patterns. All have $L_a \approx$ 48 Å according to Eq. 3. The elliptical fragments have eccentricities of 0.92 and 0.6.

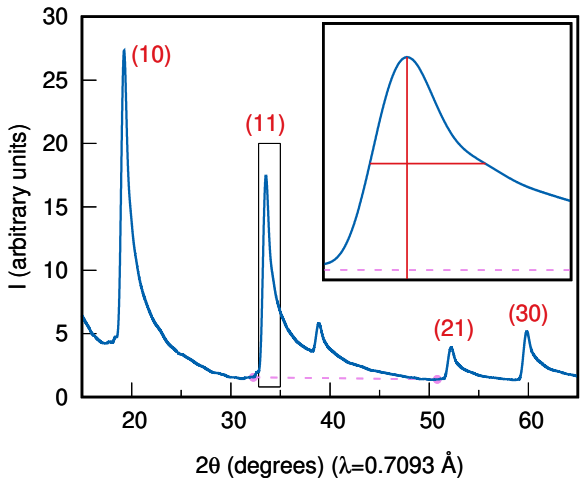

FIG. 2. Sample diffraction pattern (circle; L_a=70 Å) indicating the four peaks used. The background (dashed line) is a straight line linking the appropriate minima on either side of the peak, while θ and B correspond to the peak position and full-width-half-maximum from background, respectively.

The atom positions were used in the Debye scattering equation to generate diffraction patterns. The Debye scattering equation for a monoatomic unit cell is

$$I(Q) = f(Q)^2 \sum_{i=1}^{N} \sum_{j=1}^{N} \frac{\sin Q r_{ij}}{Q r_{ij}} \tag{4}$$

where I is the scattered intensity, f is the atomic form factor [15], N is the number of atoms, and r_{ij} the scalar distance between the i^{th} and j^{th} atoms. Q is given by

$$Q = \|\mathbf{Q}\| = \frac{4\pi \sin\theta}{\lambda} \tag{5}$$

where $\mathbf{Q}$ is the scattering vector, λ is the incident X-ray wavelength, and θ is the diffraction angle. We note that these patterns have no instrumental broadening, whereas analysis of experimentally collected patterns must account for any broadening induced by the diffractometer [16]. To simplify the Debye scattering equation for computation, instead of calculating every individual bond, the bonds are histogrammed into bins. The intensity can also be normalised to the scattering per atom. In this case, the Debye scattering equation can be expressed [17] as

$$I(Q) \approx \frac{1}{N} f(Q)^2 \left(N + 2 \sum_{k=1}^{N_{\text{bins}}} n_k \frac{\sin Q r_k}{Q r_k} \right) \tag{6}$$

where r_k is the interatomic length represented by the bin, n_k is the number of bonds in the k^{th} bin, N_{bins} is the number of bins, and N is the number of atoms. With sufficiently narrow bins, the simplified Debye diffraction equation significantly reduces computation time with little loss in diffraction intensity accuracy.

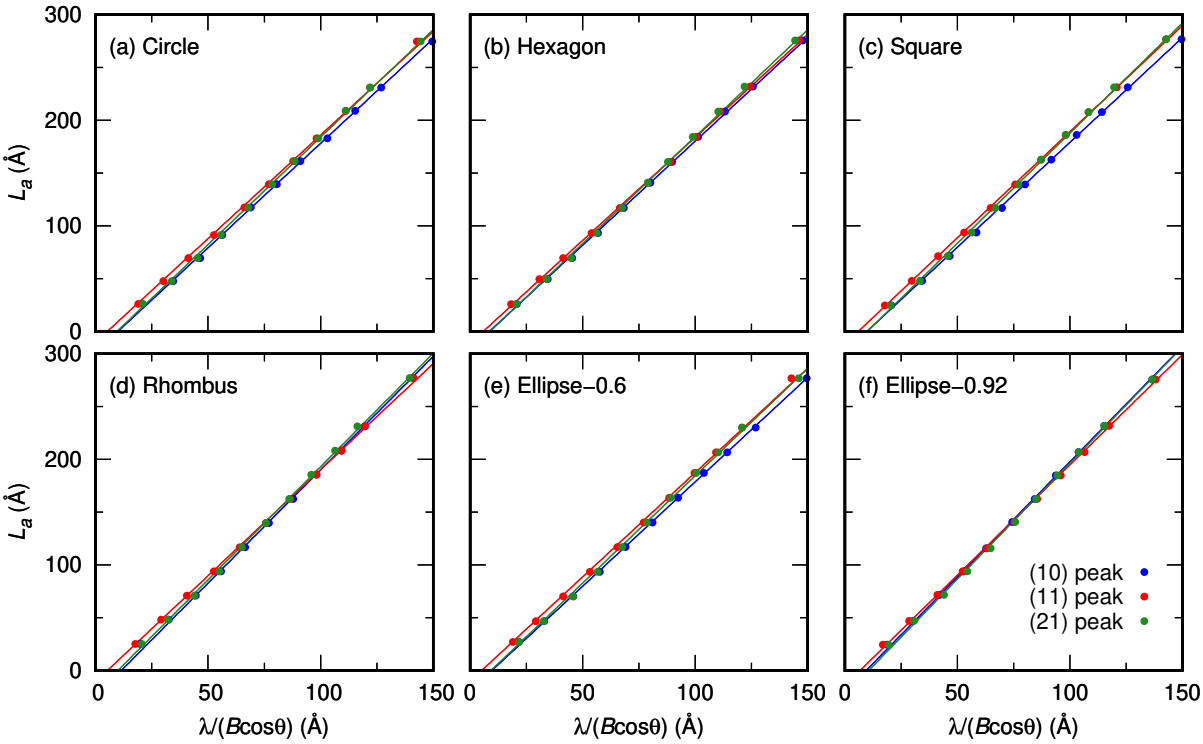

FIG. 3. Numerical data (solid circles) for all six shapes demonstrating an affine relationship between L_a and computed values of $\lambda/(B\cos\theta)$ extracted from calculated diffraction patterns. The data is well-fitted by a straight line extending out to $L_a \approx 690$ Å. Data for the (30) peak shows the same trend but is omitted for clarity.

Diffraction patterns were generated using Eq. 6 over a Q range of 1–20 Å^{-1} with a step size of 0.0005 Å^{-1} and bin intervals of 0.01 Å. Further reduction of the bin intervals had no substantive effect on the peak width or intensity. These patterns were converted to a conventional 2θ axis by setting $\lambda = 0.7093$ Å, the wavelength of molybdenum Kα radiation. This allows for the analysis of the (21) and (30) diffraction peaks, which are not normally accessible using copper Kα radiation. An example diffraction pattern is given in Fig. 2.

The (10), (11), (21), and (30) diffraction peaks of the graphene fragments were analysed to determine the factor $\lambda/(B\cos\theta)$ in the Scherrer equation. The process for determining B and θ is illustrated in the inset of Fig. 2. The value of θ is taken as the position of the peak maximum, while B is the full-width-half-maximum relative to a background indicated by the dashed line. The background was determined for each peak of interest, and was set as a straight line from the two appropriate minima to the left and right of the peak. Diffraction pattern generation and parameter extraction was carried out in MATLAB, and the numerical analysis was performed using gnuplot.

III. RESULTS

The results that form the basis of our analysis are summarized in Fig. 3. Solid circles indicate data calculated from the diffraction patterns, while the lines are straight-line regression fits to data for each peak; for clarity, data for the (30) peak is not shown. The correlation in all 24 data sets is excellent and the linearity extends to the limit of the data at $L_a \approx 690$ Å. Mathematically, this indicates that L_a and $\lambda/(B\cos\theta)$ are well-described by an affine ($y = mx + c$) relation. The values of m and c for all peak and shape combinations are summarized in Table I. The uncertainties are of order 0.01 for m and

TABLE I. Gradient, m, and y-intercept, c, of the regression fits as summarized in Fig. 3. The gradient is dimensionless, while c has units of ångströms. Shapes are listed in order of increasing eccentricity.

	m_{10}	m_{11}	m_{21}	m_{30}	c_{10}	c_{11}	c_{21}	c_{30}
Circle	1.98	1.96	2.04	1.97	−20	−10	−20	−14
Hexagon	1.97	1.95	2.03	2.00	−17	−11	−18	−15
Square	1.98	2.01	2.09	2.00	−19	−12	−21	−16
Ellipse-0.6	1.98	1.98	2.03	1.97	−19	−10	−19	−13
Rhombus	2.15	2.01	2.15	2.14	−25	−11	−22	−19
Ellipse-0.92	2.18	2.09	2.20	2.19	−21	−14	−23	−16

1 Å for c. Importantly, the data indicates that there is a statistically significant non-zero y-intercept for all shapes and peaks, with c varying between -10 and -25 Å. The Table also shows that the gradient is close to two for most situations, with only the irregular shapes showing any appreciable deviation.

The constant c in the affine relationship provides an elegant explanation for why multiple studies have observed a size-dependence in the shape factor. Specifically, the variation in K with L_a observed by Warren & Bodenstein [8] and others [9, 10] can be reproduced by fitting the data in Fig. 3 with Eq. 1 to explicitly solve for K for each value of L_a. In the absence of the parameter c, the shape factor K neccessarily varies with L_a as shown in Fig. 4, which shows the variation in K with L_a for the circle and rhombus; K is of order unity for small values of L_a, and increases monotonically to a value of approximately two for large fragments. This is precisely the variation seen in the literature and is a consequence of the affine parameter c having a negative value. Also shown in Fig. 4 are the asymptotic limits for the two well-known literature values of K (1.77 for a circle and 1.84 for a rhombus). In both cases K has been converted to its equivalent values according to our definition of L_a in Eq. 3. For large values of L_a, our analysis reproduces the literature results, confirming the validity of our simulated diffraction approach.

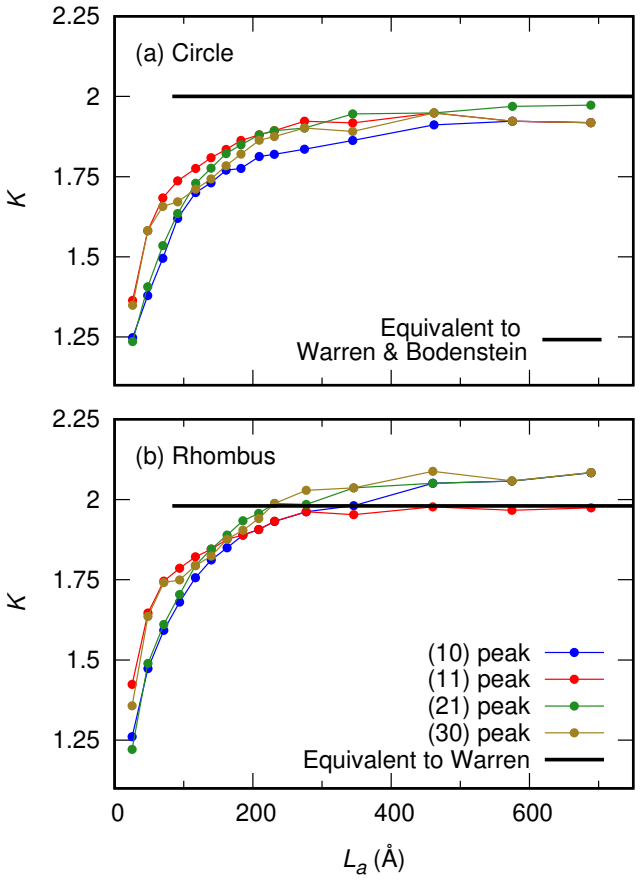

FIG. 4. Analysis of the data in Fig. 3 using a strict application of Eq. 1. The well-known size-dependency effect [8–10] is reproduced. Equivalent values for the shape factors using our definition of L_a (Eq. 3) are shown as black lines.

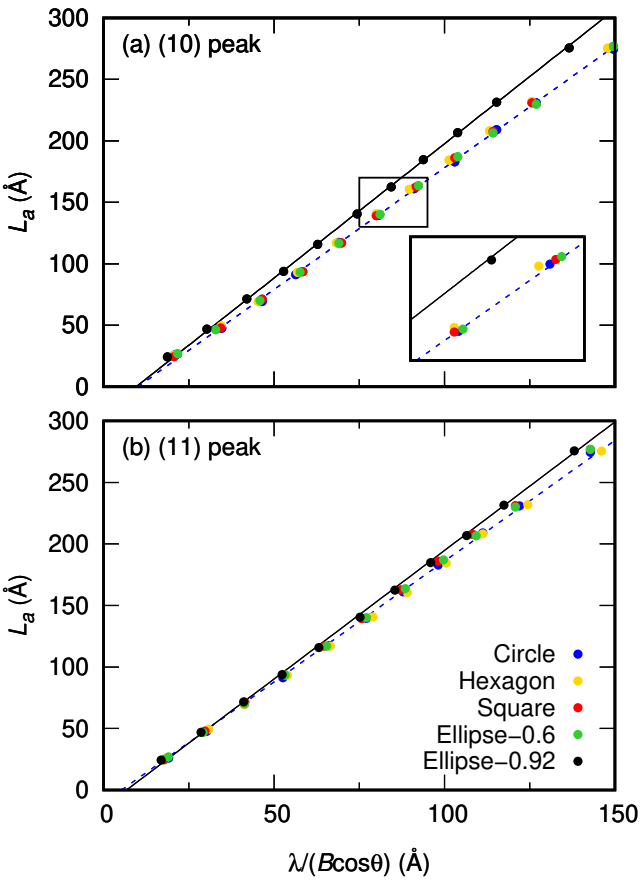

FIG. 5. Same data as Fig. 3, except grouped by peak instead of shape. The dashed line is an affine fit to the data for circles. All plotted data falls onto this line, except for the more eccentric ellipse. The inset in panel (a) highlights this behaviour. For clarity, data for the rhombus is not shown.

The merit of our area-based definition of L_a is demonstrated in Fig. 5. Here we replot the data in Fig. 3, this time grouping by peak. It can be seen that the data for the regular polygons and the low-eccentricity ellipse effectively lie on a universal line, with only the highly eccentric ellipse showing any significant deviation. Data for the rhombus (not shown) lies midway between these two groups. The (21) and (30) peaks exhibit the exact same behaviour, showing that these trends are not specific to any particular layer shape or peak. Close inspection of Table I reveals the same trends seen in Fig. 5 in the form of clustering of m and c for each peak. Prior to selecting Eq. 3 as our definition of L_a, we also explored an alternative form, $L_a = 4 \times$ area/perimeter, which is conceptually similar to the definition for circles by Warren & Bodenstein [6]. Although we still observed an affine rela-

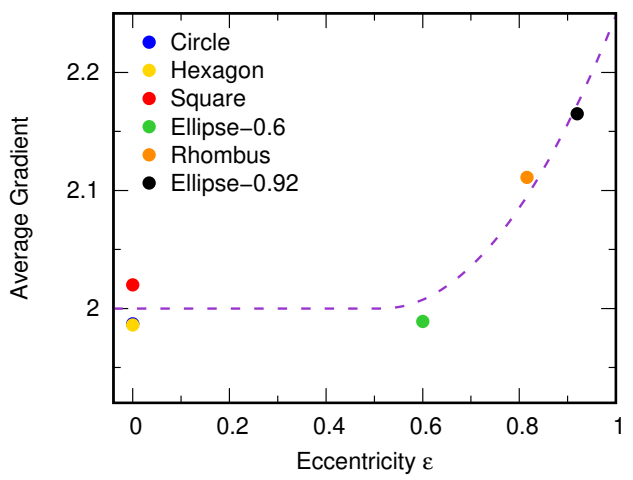

FIG. 6. Average gradient of the affine fit as a function of eccentricity for the six shapes. Averages are computed using all four peaks in Table I, and the standard-error-in-the-mean is similar to the size of the filled circles. The dashed line is a piecewise continuous function (constant of two linked to a quadratic) to guide the eye.

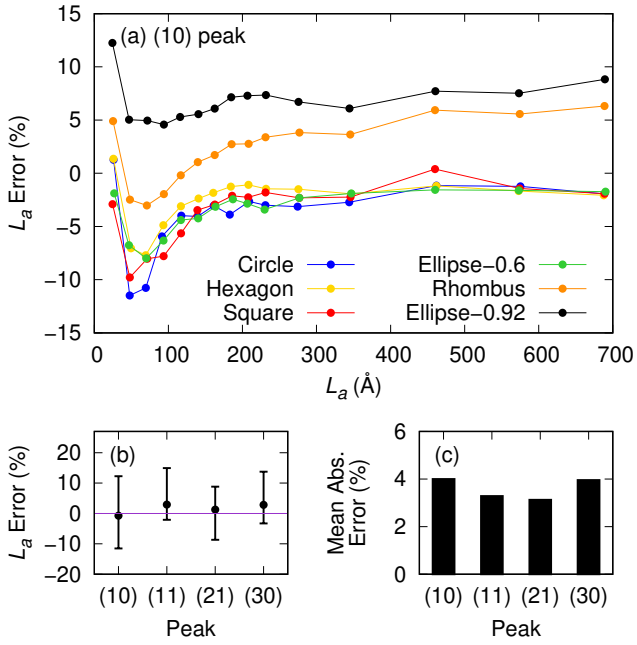

FIG. 7. Error associated with Eq. 7 and the recommended values of K'=2 and c=−16 Å. Panel (a) shows the error in L_a for the (10) peaks spanning all fragment sizes and shapes. Panel (b) shows the mean error (dots) and range of errors (bars) for each peak. Panel (c) shows the average value of the absolute error for all data of each peak.

tionship for all shapes and peaks, there was considerable spread in the m and c values, and the data for different shapes did not coincide on a universal line.

The universal behaviour for regular shapes seen in Fig. 5 can be usefully understood by comparing the eccentricity to the average gradient for each shape as computed using the data for the four peaks in Table I. The data in Fig. 6 shows that a average gradient of two applies for a wide range of shapes. Only for the rhombus and the more eccentric ellipse does the gradient begin to deviate, and even then, the trend is monotonic. As noted earlier, the literature values of K=1.84 for the rhombus and K=1.77 for the circle are equivalent to 1.98 and 2.00 with our area-based definition. This convergence of values provides ample justification for proposing a revised Scherrer equation for L_a of the form:

$$L_a = K' \frac{\lambda}{B \cos\theta} + c \qquad (7)$$

where K'=2 and c is a constant to be determined. Fitting simultaneously to the three regular polygons (circle, hexagon, square) yields a value of −16 Å, similar to the values of c in Table I.

While one could conceive of a Scherrer equation with values of K' and c specific to each peak, from a practical point of view it is preferable to use K'=2 and c=−16 Å for all situations. To quantify the error that this introduces, we reanalyzed our data using Eq. 7 and compared each predicted value of L_a to the actual value for the fragment. The percentage error for each shape and size is shown in Fig. 7(a) for the (10) peak. Even though the values of K' and c are not optimized to any particular peak or shape, the error introduced by Eq. 7 is never greater than 15%, and for large fragments with uniform shape is typically only a few percent.

The scatter of the entire data set in Fig. 7(a) is summarized in a single data-point for the (10) peak in panel (b). The bars indicate the range of the error about the mean, where all the data in panel (a) is utilized. The remaining data-points in panel (b) show that the trends for the other three peaks resemble the (10) peak, with a similar range of errors and a mean close to zero. The average of the absolute errors provides a useful metric to evaluate the accuracy of Eq. 7. Panel (c) shows that the mean absolute error is only a few percent. Note that for typical diffraction measurements using copper Kα radiation, the most important two peaks are the (10) and (11), for which the mean error in panel (b) is just −1.2% and +2.8%, respectively.

To put these numbers into perspective, the size-dependence implicit in the conventional Scherrer equation introduces an effective uncertainty of nearly 100% due to the variation of K between 1.1 and 2.0. Furthermore, there is considerable variation in the literature regarding the appropriate choice of K, to which is added an ambiguous definition of L_a. As shown by Warren & Bodenstein [8], the choice of diffraction peak can also alter K by around 30%. All of these problems are resolved with our area-based definition of L_a together with the use of an additive constant in the Scherrer equation. While we don't have a physical explanation for why this modi-

fication is so successful, the empirical support for such a term is strong. Due to the negative additive constant, our proposed modification will necessarily fail for extremely small values of $\lambda/(B\cos\theta)$. The onset of breakdown can be seen in Fig. 7(a) where the affine relationship begins to change for the smallest L_a values of 25 Å and below this value we do not recommend the use of our coefficients. In practice, we do not expect this lower limit to be a significant issue, as genuine graphitic structures with L_a below 30 Å have not been found, and in the words of Ref. [14], "*will probably never be*".

In summary, we have studied 2D graphene fragments of various shapes and sizes by analysing simulated X-ray diffraction patterns. The layer size of the graphene fragments varied between 25 and 690 Å and was defined as the square-root of the area. For all diffraction peaks over the entire size-range, a strong affine relationship was found between L_a and the Scherrer quantity $\lambda/(B\cos\theta)$. Deviations in the gradient correlate with an increase in the eccentricity of the fragment. To preserve this affine relationship, we modify the Scherrer equation to include an emprical additive constant. Fitting to the principal peaks of the regular shapes yields the expression $L_a = 2\lambda/(B\cos\theta) - 16$, where the layer size is in ångströms.

Our analysis also provides an explanation for a size-dependency problem reported in the literature for the conventional Scherrer equation, which assumes c=0. Futhermore, the area-based definition of L_a is easy to interpret, improving on previous approaches that were either algebraically complex or shape-specific. It also results in universal behaviour whereby data for regular shapes falls on a common line.

The simplicity of our computational approach suggests other areas where a similar approach can be applied. For example, it would be valuable to revisit the data of Fujimoto [9] and Dopita *et al.* [10] to test whether an affine relationship exists for L_c in their stacked graphitic layer systems. It would also be straightforward to study curvature by bending the graphene layers cylindrically or by introducing pentagons and/or heptagons. Aside from carbon, there are also many other analogous 2D and layered-2D materials such as boron nitride, phosphorene, and MoS_2, where a robust measure of L_a would be valuable.

ACKNOWLEDGEMENTS

Helpful discussions with Alec Duncan and Irene Suarez-Martinez are gratefully acknowledged.

APPENDIX

It has been shown by Warren [3], and noted by Fujimoto [9] and Dopita *et al.* [10], that the position of the peak maximum of an (hk) reflection and the position of the same reflection calculated from crystallographic parameters do not exactly coincide. Although this does not affect our calculations of L_a in any meaningful way, the differences should be taken into account when calculating unit cell parameters, especially for small layer sizes. The shift in peak position can be represented by

$$\Delta(\sin\theta) = \sin\theta_{\text{max.}} - \sin\theta_{\text{cryst.}} = \frac{U\lambda}{L_a + V} \qquad (8)$$

where λ is the wavelength, U and V are empirical parameters and the position of the peak maximum and crystallographic peak are given by $\sin\theta_{\text{max.}}$ and $\sin\theta_{\text{cryst.}}$, respectively. Values of U and V for each of the shapes and reflections are listed in Table II, where L_a in Eqn. 8 is calculated from the corresponding values in Table I. In an experimental setting the shape will not be known, and hence it is preferable to calculate the layer size using Eqn. 7 with K'=2 and c=−16 Å. Fitting simultaneously to the (10), (11), and (21) peaks of the three regular polygons, yields U=0.156 and V=9.9 Å. These values allow for the accurate determination of unit cell parameters for carbons over a wide range of layer size.

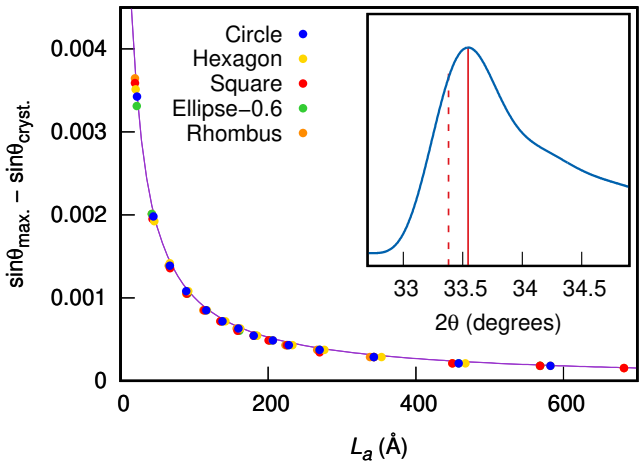

FIG. 8. Shift in the position of the (11) peak maximum (solid line in inset) with respect to the position of the reflection calculated with crystallographic parameters (dashed line in inset). All peaks and shapes show the same relationship. L_a was calculated from the diffraction data using Eqn. 7 with K'=2 and c=−16 Å. The continuous line represents a fit through the data for the regular shapes.

TABLE II. Values of U and V, as defined in Eqn. 8, of the regression fits outlined in Fig. 8. The value of L_a used in the regression was calculated using Eqn. 7 with the corresponding values from Table I. U is dimensionless, while V has units of ångströms. Shapes are listed in order of increasing eccentricity.

	U_{10}	U_{11}	U_{21}	U_{30}	V_{10}	V_{11}	V_{21}	V_{30}
Circle	0.161	0.145	0.160	0.146	16.0	2.9	10.2	4.8
Square	0.155	0.149	0.159	0.143	13.0	6.0	10.0	4.6
Hexagon	0.155	0.146	0.156	0.143	13.2	5.2	10.5	5.1
Ellipse-0.6	0.153	0.146	0.155	0.145	12.1	4.0	8.4	4.3
Rhombus	0.142	0.146	0.151	0.133	14.3	3.6	6.6	8.1
Ellipse-0.92	0.160	0.124	0.141	0.153	14.9	7.6	12.1	7.0

[1] L. G. Cançado, K. Takai, T. Enoki, M. Endo, Y. A. Kim, H. Mizusaki, A. Jorio, L. N. Coelho, R. Magalhães Paniago, and M. A. Pimenta, "General equation for the determination of the crystallite size la of nanographite by raman spectroscopy," Appl. Phys. Lett. **88**, 163106 (2006).

[2] P. Scherrer, "Bestimmung der grösse und der inneren struktur von kolloidteilchen mittels röntgenstrahlen," Nachr. Ges. Wissenschaft. Göttingen **3**, 98–100 (1918).

[3] B. E. Warren, "X-ray diffraction in random layer lattices," Phys. Rev. **59**, 693–698 (1941).

[4] W.L. Bragg, *A General Survey*, The Crystalline State, Vol. 1 (G. Bell and Sons Ltd, London, 1933) p. 189.

[5] J. Biscoe and B. E. Warren, "An x-ray study of carbon black," J. Appl. Phys. **13**, 364–371 (1942).

[6] B. E. Warren and P. Bodenstein, "The shape of two-dimensional carbon black reflections," Acta Crystallogr. **20**, 602–605 (1966).

[7] N. Iwashita, C. R. Park, H. Fujimoto, M. Shiraishi, and M. Inagaki, "Specification for a standard procedure of x-ray diffraction measurements on carbon materials," Carbon **42**, 701–714 (2004).

[8] B. E. Warren and P. Bodenstein, "The diffraction pattern of fine particle carbon blacks," Acta Crystallogr. **18**, 282–286 (1965).

[9] H. Fujimoto, "Theoretical x-ray scattering intensity of carbons with turbostratic stacking and ab stacking structures," Carbon **41**, 1585–1592 (2003).

[10] M. Dopita, M. Rudolph, A. Salomon, M. Emmel, C. G. Aneziris, and D. Rafaja, "Simulations of x-ray scattering on two-dimensional, graphitic and turbostratic carbon structures," Adv. Eng. Mater. **15**, 1280–1291 (2013).

[11] P. Debye, "Zerstreuung von röntgenstrahlen," Ann. Phys. **351**, 809–823 (1915).

[12] R. Diamond, "X-ray diffraction data for large aromatic molecules," Acta Crystallogr. **10**, 359–364 (1957).

[13] W. Ruland and B. Smarsly, "X-ray scattering of non-graphitic carbon: an improved method of evaluation," J. Appl. Crystallogr. **35**, 624–633 (2002).

[14] Pascal Puech, Agnieszka Dabrowska, Nicolas Ratel-Ramond, Gérard L. Vignoles, and Marc Monthioux, "New insight on carbonisation and graphitisation mechanisms as obtained from a bottom-up analytical approach of x-ray diffraction patterns," Carbon **147**, 602 – 611 (2019).

[15] D. Waasmaier and A. Kirfel, "New analytical scattering-factor functions for free atoms and ions," Acta Crystallogr. A **51**, 416–431 (1995).

[16] R. W. Cheary and A. Coelho, "A fundamental parameters approach to x-ray line-profile fitting," J. Appl. Crystallogr. **25**, 109–121 (1992).

[17] M. Wojdyr, "Debyer," https://debyer.readthedocs.io/en/latest/.